

SPIN-POLARIZED SURFACE POSITRONIUM SPECTROSCOPY — CURRENT STATUS AND FUTURE*

A. KAWASUSO, M. MAEKAWA

National Institute for Quantum Science and Technology
1233, Watanuki, Takasaki, Gunma, 370-1292, Japan

*Received 31 October 2023, accepted 29 November 2023,
published online 26 February 2024*

Spin-polarized surface positronium (Ps) spectroscopy is a new method to characterize the spin-polarized electronic states associated with the top-surface of solid. We have been developing this method based on the Ps time-of-flight technique with a transversely spin-polarized positron beam generated with a ^{22}Na source. Although the spin-polarized density of states (DOS) of Ni(111) and Co(0001) surfaces were successfully obtained, there was still room for improvement in the energy resolution and count rate. Subsequently, we inserted a Ps quencher (Kapton) at the detector position so that more Ps atoms were captured in a reduced time (and hence energy) window. Consequently, the energy resolution and count rate were improved by an order of magnitude, giving rise to much better spin-polarized DOS profile. In the future, to obtain further information about the band dispersion and the Fermi surface of solid top-surface, this method needs to be extended to the angle-resolvable version. In this respect, we discuss the possibility of positron emission tomography technology.

DOI:10.5506/APhysPolBSupp.17.1-A4

1. Introduction

To settle the problems of current electronic devices, such as the energy consumption and the plateau of performance, the so-called spintronics research field has emerged in the last decade [1]. New concepts and principles found in the fundamental solid-state physics, such as the novel spin phenomena occurring at the surface and interface [2] and the discovery of a new class of topological materials [3, 4] would be the foundation of technological innovation. Today, vast materials and phenomena related to spin generation, manipulation, and transport are extensively studied [5].

* Presented at the Symposium on *New Trends in Nuclear and Medical Physics*, Kraków, Poland, 18–20 October, 2023.

In the fundamental research of spintronics materials, the observation of top-surface electronic states is an important task. Photoemission spectroscopy has been widely and successfully used leading to many outstanding works. However, this method hardly observes the top-surface layer alone, because photoelectrons are emitted not only from the top-surface layer but also from deeper layers. Due to this drawback, for example, the spin-polarization induced into graphene via the magnetic proximity effect has not been fully revealed by photoemission spectroscopy [6].

Surface positronium (Ps) spectroscopy reported here has an extremely high surface sensitivity and might play a complementary role to photoemission spectroscopy. Especially, the ‘spin-polarized’ version using spin-polarized positron beam would be a precious method to determine the spin state of the top-surface layer. The prototype was demonstrated by the Michigan group already in 1982 [7]. However, afterwards to date, this method has been neither used nor developed. We revived this old and new method [8–13] considering the recent rapid progress of spintronics research mentioned above. In this paper, we introduce the principle of this method, some of our achievements so far, and discuss the future prospects.

2. Principle of surface Ps spectroscopy

Ps is the hydrogen-like bound state of an electron and a positron. Depending on the mutual spin direction of the electron and positron, the spin-singlet state ($S = 0$) and spin-triplet state ($S = 1$) are available. These self-annihilation lifetimes in vacuum are 125 ps ($S = 0$) with two-gamma decay and 142 ns ($S = 1$) with three-gamma decay. In many cases, three-gamma annihilation events of long-lived spin-triplet Ps are used in the Ps spectroscopy. With a few exceptions, Ps is not formed in the bulk of solid due to the screening of the Coulomb interaction between a positron and an electron [14–16]. Hence, the Ps formation can occur only at the top-surface layer, where the screening effect is adequately reduced. Positrons implanted into solid, after thermalization, diffuse back to the surface/vacuum interface and a part of them are emitted into vacuum as Ps atoms by picking up electrons at the top-surface layer as schematically shown in Fig. 1 (a) [17, 18]. The prerequisite of spontaneous Ps emission is the negative Ps formation potential given by $\Phi_{\text{Ps}} = \phi_- + \phi_+ - E_{\text{B}} < 0$, where ϕ_- and ϕ_+ are the electron and positron work functions, respectively, and E_{B} is the Ps binding energy in vacuum ($= 6.8$ eV). As shown in Fig. 1 (b), positrons can pick up electrons in the occupied states from the Fermi level (E_{F}) to the depth of $-\Phi_{\text{Ps}}$. The maximum and zero Ps energies correspond to these two electron energy levels. Depending on the electron momentum, the emitted Ps atoms may also have a certain angular distribution (Fig. 1 (c)). The Ps energy and

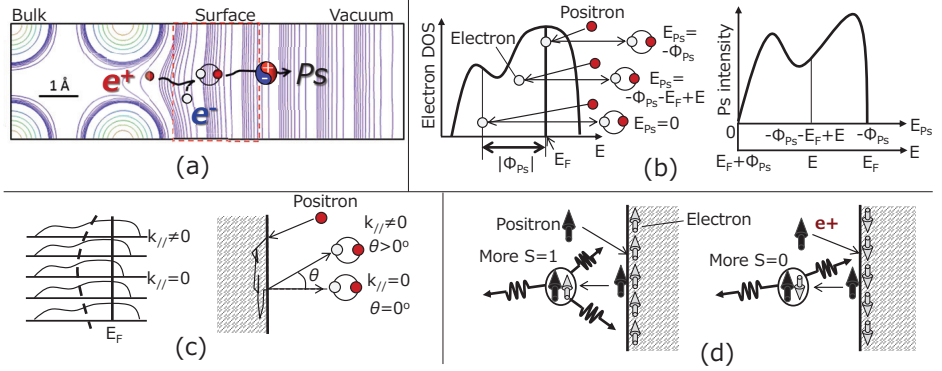


Fig. 1. Schematic representations of (a) surface Ps emission, (b) relationship between electron density of states (DOS) and Ps kinetic energy distribution, (c) relationship between band dispersion and Ps angular distribution and (d) spin-dependent surface Ps emission.

angular distributions might express the electron density of states (DOS) and the band dispersion, respectively, although, even in the simplest case, these are given by the golden rule formula including the positron and electron wave functions and transition matrix under the energy and momentum conservations [19, 20]. When both positrons and electrons are spin-polarized, generated Ps atoms are also spin-polarized. Hence, as shown in Fig. 1 (d), by reversing the mutual polarization direction of positrons and electrons, the fractions of $S = 0$ and $S = 1$ states can be changed and thereby the spin-polarization of surface electrons is determined as

$$P_-(E_{Ps}) = \frac{1}{P_+} \frac{2\epsilon(1) + \epsilon(0)}{2\epsilon(1) - \epsilon(0)} \frac{F_{\uparrow\downarrow}(E_{Ps}) - F_{\uparrow\uparrow}(E_{Ps})}{F_{\uparrow\downarrow}(E_{Ps}) + F_{\uparrow\uparrow}(E_{Ps})}, \quad (1)$$

where P_+ denotes the positron spin polarization, E_{Ps} denotes the Ps energy, $F_{\uparrow\uparrow, \uparrow\downarrow}(E_{Ps})$ denotes the Ps fraction obtained under the parallel–antiparallel spin conditions, and $\epsilon(1) = 0.3$ and $\epsilon(0) = 0.4$ denote the detection efficiencies for annihilation gamma rays from the Ps atoms with magnetic quantum numbers of ± 1 and 0, respectively [21].

3. Current status of spin-polarized surface Ps spectroscopy

In this section, we first introduce the simplest spin-polarized surface Ps spectroscopy without energy resolution and its application to the study of magnetic proximity effect on graphene. Subsequently, we report on the further development of spin-polarized surface Ps spectroscopy with energy resolution.

3.1. Spin-polarized surface Ps spectroscopy without energy resolution

In the case that the change in total positronium fraction upon spin reversal is simply observed, the spin-polarization is given by integrating Eq. (1) with respect to E_{Ps} . The Michigan group conducted such an analysis using annihilation lifetime measurement [7]. Instead of this, we used the energy spectrum of annihilation gamma rays [22–26]. Figure 2(a) shows the schematic drawing of the apparatus. Transversely spin-polarized positron beam with typical energy of ~ 10 keV is implanted into in-plane magnetized sample. Figure 2(b) shows the relative change in the Ps fraction upon reversal of magnetization direction obtained for Fe, Co, and Ni polycrystals [27]. This result confirms the detection of spin-polarized surface electrons.

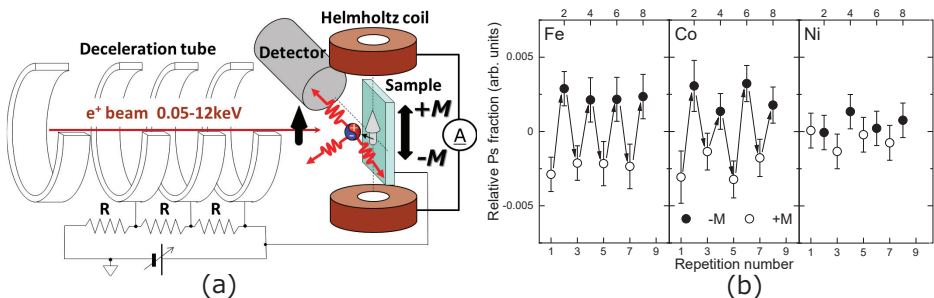


Fig. 2. (a) Schematic representation of the spin-polarized surface Ps spectroscopy experiment: transversely spin-polarized positron beam (12 keV) is decelerated and implanted into a sample magnetized by external coils. Annihilation gamma rays of the emitted Ps atoms are detected by a detector (typically a pure Ge detector). (b) Change in a relative Ps fraction (arb. units) upon field reversal obtained for the Fe, Co, and Ni polycrystals.

We extended the above way to the detection of spin polarization of graphene and h-BN on ferromagnets [25, 26]. Here, we pick up the results for graphene on Co(0001), Ni(111), and $\text{Co}_2\text{Fe}(\text{GaGe})_{0.5}(001)$. The lattice matching of graphene with Co(0001) and Ni(111) are exceptionally good and hence graphene is coherently bound on these surfaces. Whereas, due to the bad lattice matching, graphene is only weakly bound on the $\text{Co}_2\text{Fe}(\text{GaGe})_{0.5}(001)$ surface mainly via the van der Waals force. Figure 3 shows that graphene is well spin-polarized by Co and Ni, while almost null spin-polarization is induced from $\text{Co}_2\text{Fe}(\text{GaGe})_{0.5}$ to graphene. Our theoretical calculation indicated that graphene is well spin-polarized by Co and Ni due to the strong π - d hybridization between graphene and these metals. One concern is that due to the strong hybridization, the Dirac cone dispersion which is the inherent characteristics of graphene is lost [25]. Also, weak

hybridization between graphene and $\text{Co}_2\text{Fe}(\text{GaGe})_{0.5}(001)$ was shown to be insufficient to induce spin polarization into graphene, while the Dirac cone dispersion of graphene is predicted to be preserved [26].

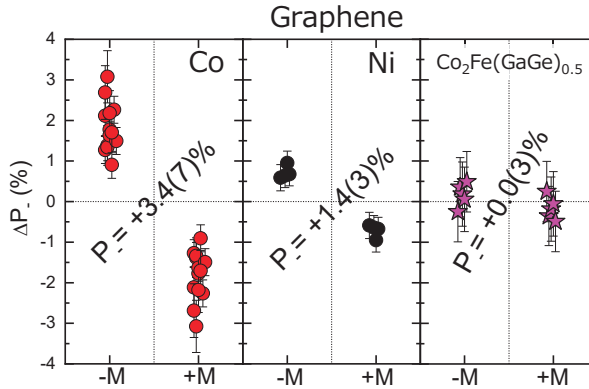


Fig. 3. Spin polarizations for single layer graphene on the $\text{Co}(0001)$, $\text{Ni}(111)$, and $\text{Co}_2\text{Fe}(\text{GaGe})_{0.5}(001)$ surfaces obtained by spin-polarized surface Ps spectroscopy.

Thus, spin-polarized surface Ps spectroscopy revealed the above-mentioned picture about the magnetic proximity effect on graphene, thanks to the extremely high surface selectivity, and will complement the results obtained by photoemission spectroscopy.

3.2. Spin-polarized surface Ps spectroscopy with energy resolution

The obtained spin polarization described in the preceding subsection is only an average of all electrons picked up by positrons. To obtain spin-polarization depending on the electron energy level, *i.e.*, spin-polarized DOS, we further developed a Ps time-of-flight measurement system as shown in Fig. 4(a) [13]. Transversely spin-polarized positron beam is incident on in-plane magnetized sample. The positron incidence is tagged by secondary electrons detected using the channeltron device. The annihilation gamma rays from the Ps atoms generated at the sample surface are detected by NaI scintillation detectors through a narrow lead slit. From the time difference between positron incidence and Ps annihilation events, the Ps time-of-flight spectrum is acquired. The estimated energy resolution was 0.8 eV at $E_{\text{Ps}} = 3$ eV and the count rate was measured to be ~ 0.1 cps with the geometry of Fig. 4(a). Figure 4(b) (upper panels) shows the $P_{-}(E_{\text{Ps}})$ profiles (see, Eq. (1)) determined for $\text{Co}(0001)$ and $\text{Ni}(111)$ surfaces as a function of $E_{\text{Ps}} + \Phi_{\text{Ps}}$. That is, $F_{\uparrow\uparrow}(E_{\text{Ps}})$ and $F_{\uparrow\downarrow}(E_{\text{Ps}})$ are the Ps energy spectra for positive and negative magnetization directions, respectively, as defined in Fig. 2(a). The horizontal axis is directly comparable to the electron energy

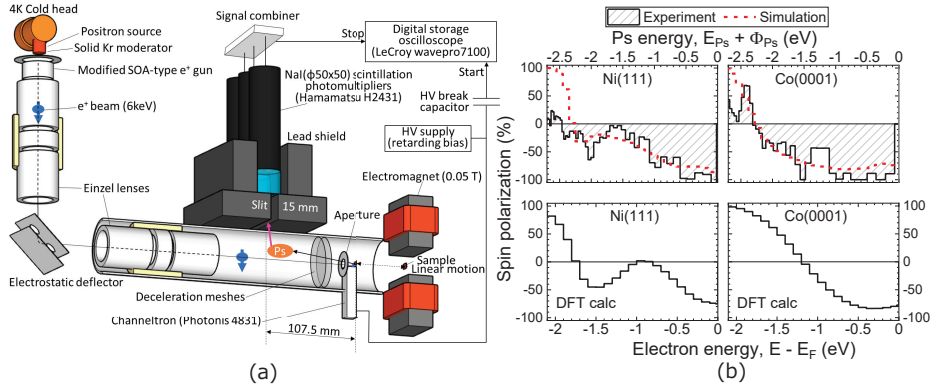


Fig. 4. (a) Schematic representation of the time-of-flight-based spin-polarized surface Ps spectroscopy apparatus. (b) (upper two panels) $P_-(E_{Ps})$ as a function of $E_{Ps} + \Phi_{Ps}$ obtained for the Ni(111) and Co(0001) surfaces with the apparatus in (a), and (b) (lower two panels) the spin-polarized DOSs by the DFT calculation. Dashed curves in the upper two panels are the $P_-(E_{Ps})$ simulated with these DFT profiles and system energy resolution function.

$E - E_F$. Large negative spin polarizations were observed below the Fermi level ($E_{Ps} + \Phi_{Ps} < 0$). These are in good agreement with the simulation curves considering the spin-polarized DOS obtained by the density functional theory (DFT) calculation in Fig. 4(b) (lower panels) and the energy resolution function of the system.

To improve both the energy resolution and the count rate, we further modified the apparatus by inserting a Ps quencher (Kapton film) at the detector position as schematically shown in Fig. 5(a). Most Ps atoms passing through the slit region in the original configuration may be captured

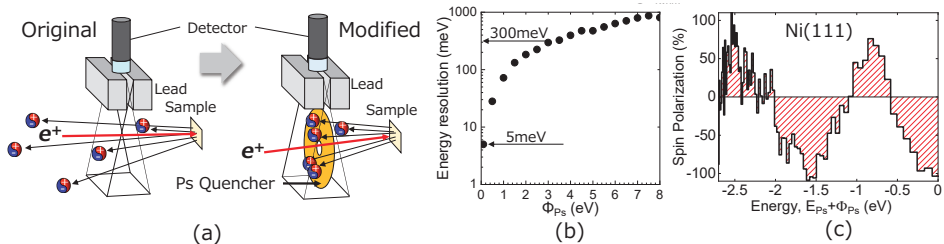


Fig. 5. (a) Schematic representations of the original configuration (left) and modified configuration with Ps quencher (right) around the lead-slit detector section in the apparatus shown in Fig. 4(a). (b) Energy resolution estimated for the modified configuration in (a) as a function of Ps energy. (c) Spin-polarized DOS profile obtained for the Ni(111) surface in the modified configuration in (a).

by the quencher in a reduced time and hence energy windows. Figure 5(b) shows the estimated energy resolution as a function of E_{Ps} . It is 0.3 eV at $E_{\text{Ps}} = 3$ eV and 5 meV at $E_{\text{Ps}} = 100$ meV. The count rate got to 1 cps. Consequently, we obtained the $P_-(E_{\text{Ps}})$ profile for Ni(111) as shown in Fig. 5(c), which is much better than the previous one (Fig. 4(b)). (Though the energy dependence of quenching rate is not clear, this effect is cancelled as seen in Eq. (1).)

4. Future prospects

As mentioned above, the electron spin-polarization of the top-surface layer depending on the electron energy level has been acquirable by spin-polarized surface Ps spectroscopy. Nevertheless, the angle-resolved measurement has not yet been established. The further improvement of energy resolution and count rate should also be pursued for high-quality data acquisition. As for the high-energy resolution measurement, the time-of-flight measurement of Ps excited to the high Rydberg states by laser illumination was shown to be one potential way owing to the elongation of Ps lifetime [28, 29]. Apart from this, high-efficiency and angle-resolved measurement might be feasible in the Ps in-flight annihilation measurement using an omnidirectional detector system such as positron emission tomography (PET). That is, the replacement of conventional lead-slit detectors in the traditional time-of-flight system with the PET system with long enough axial detectors as the J-PET developed by the Jagiellonian University [30–32]. Here, we discuss the feasibility, though based on rough and preliminary estimation.

Figure 6(a) shows the simulated annihilation event distribution of spin-triplet Ps in an axial symmetric condition. A step-like positron energy distribution from 0 to 5 eV is assumed. The angular distribution is a Gauss function with the half-width of 90 degrees. The beam profile is a two-dimensional Gauss function with the half-width of 6 mm. From this simulation, most annihilation events occur in the space shown in Fig. 6(a) and hence the inner diameter and length of the cylindrical PET detector of both 300 mm may be ample enough. The energy resolution was simply estimated as $\Delta E = m[(\frac{r+\Delta r/2}{t-\Delta t/2})^2 - (\frac{r-\Delta r/2}{t+\Delta t/2})^2]$, where m denotes the electron rest mass, r and t denote the flight length and time of Ps, respectively, and Δr and Δt are the spatial and time resolutions of the total system, respectively. We assumed $\Delta r = 1$ mm and $\Delta t = 500$ ps. The latter may be feasible in the current PET systems using plastic and LSO scintillators. The former may not be feasible in conventional PET systems with large field of view. However, $\Delta r = 1$ mm is probably crucial for maintaining a high-energy resolution measurement. Hopefully, this prerequisite can be fulfilled by reducing the sizes of scintillator and field of view. Figure 6(b) shows the

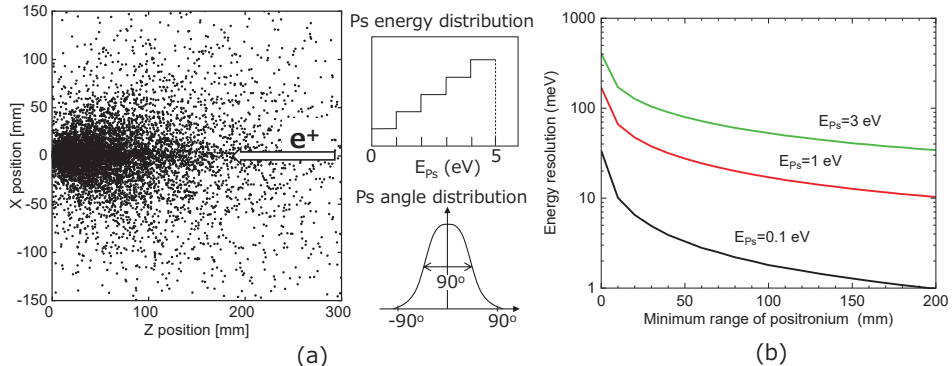


Fig. 6. (a) Annihilation event distribution of spin-triplet Ps emitted from the sample surface simulated with Ps energy and angular distributions shown at the right-hand side of the figure. The positron beam is incident on a sample as indicated by the arrow. The beam profile is assumed to be a two-dimensional Gauss function with the half-width of 6 mm. The sample surface is located at $x = 0$. (b) Energy resolution estimated for various Ps energies as a function of minimum range of Ps to be collected.

estimated energy resolution for several Ps energies as a function of minimum Ps range to be collected. The minimum range means the distance from the sample surface, *e.g.*, the minimum range of zero corresponds to the sample surface. The maximum range is assumed to be 300 mm. The energy resolution becomes better by collecting Ps annihilation events with longer flight distance, while the amount of collected Ps (*i.e.*, count rate and efficiency) decreases. Assuming 20% efficiency, the minimum range varies from 30 mm ($E_{Ps} = 100$ meV) to 140 mm ($E_{Ps} = 3$ eV). The angular resolution was also simply estimated as $\Delta\theta = \tan^{-1}(\frac{\Delta r/2}{vt})$, where v denotes the Ps velocity. Thus, the energy resolution and angular (momentum) resolution are 5 meV and 0.66° (0.0013 \AA^{-1}) for $E_{Ps} = 0.1$ eV, 17 meV and 0.22° (0.0014 \AA^{-1}) for $E_{Ps} = 1$ eV, and 42 meV and 0.19° (0.0019 \AA^{-1}) for $E_{Ps} = 3$ eV. The angular resolution is good enough for instance for the Fermi surface mapping. Although the energy resolution is not as good as that of state-of-the-art photoemission spectroscopy, it is comparable to that obtained in the laser excitation-assisted Ps time-of-flight method and hence a lot of applications of surface Ps spectroscopy may be possible.

5. Summary

We have demonstrated the superiority of spin-polarized surface Ps spectroscopy in the determination of spin-polarization of the solid top-surface layer through some practical applications. We further demonstrated that

the Ps time-of-flight method is able to observe the spin-polarized DOS of the top-surface layer. For extending spin-polarized surface Ps spectroscopy to both angle- and energy-resolved version, some innovation is necessary. Considering the fact that the J-PET system is successfully used for the test of symmetry in the electromagnetic interaction through the observation of Ps annihilation events, we preliminary examined the feasibility of omnidirectional measurement of annihilation gamma rays using the PET system. At present, the spatial resolution as high as possible should be the key. The further progress in PET technology may also open new applications in both nuclear/particle physics and materials science.

REFERENCES

- [1] J. Puebla, J. Kim, K. Kondou, Y. Otani, *Commun. Mater.* **1**, 24 (2020).
- [2] F. Hellman *et al.*, *Rev. Mod. Phys.* **89**, 025006 (2017).
- [3] Y. Ando, *J. Phys. Soc. Jpn.* **82**, 102001 (2013).
- [4] N.P. Armitage, E.J. Mele, A. Vishwanath, *Rev. Mod. Phys.* **90**, 015001 (2018).
- [5] A. Hirohata *et al.*, *J. Magn. Magn. Mater.* **509**, 166711 (2020).
- [6] S.J. Gilbert, P.A. Dowben, *J. Phys. D: Appl. Phys.* **53**, 343001 (2020).
- [7] D.W. Gidley, A.R. Köymen, T.W. Capehart, *Phys. Rev. Lett.* **49**, 1779 (1982).
- [8] A. Kawasuso, M. Maekawa, *Appl. Surf. Sci.* **255**, 108 (2008).
- [9] M. Maekawa *et al.*, *Nucl. Inst. Meth. Phys. Res. B* **308**, 9 (2013).
- [10] M. Maekawa *et al.*, *J. Phys.: Conf. Ser.* **505**, 012033 (2014).
- [11] M. Maekawa, H. Zhang, H. Li, A. Kawasuso, *Jpn. J. Appl. Phys. Conf. Proc.* **2**, 011305 (2014).
- [12] M. Maekawa, K. Wada, A. Miyashita, A. Kawasuso, *J. Phys.: Conf. Ser.* **791**, 012009 (2017).
- [13] M. Maekawa *et al.*, *Phys. Rev. Lett.* **126**, 186401 (2021).
- [14] A. Held, S. Kahana, *Can. J. Phys.* **42**, 1908 (1964).
- [15] H. Kanazawa, Y.H. Ohtsuki, S. Yanagawa, *Phys. Rev.* **138**, A1155 (1965).
- [16] B. Barbiellini, P.M. Platzman, *Phys. Stat. Solidi C* **6**, 2523 (2009).
- [17] P.J. Schultz, K.G. Lynn, *Rev. Mod. Phys.* **60**, 701 (1988).
- [18] A.P. Mills, «Positron and Positronium Emission Spectroscopy», in: A. Dupasquire, A.P. Mills (Eds.) «Positron Spectroscopy of Solids», IOS Press, Ohmsha, Amsterdam, Oxford, Tokyo, Washington DC 1993.
- [19] A. Ishii, *Sol. Stat. Phen.* **28-29**, 213 (1992).
- [20] A.P. Mills, L. Pfeiffer, P.M. Platzman, *Phys. Rev. Lett.* **51**, 1085 (1983).
- [21] R.M. Drisko, *Phys. Rev.* **102**, 1542 (1956).

- [22] A. Kawasuso *et al.*, *J. Mag. Mag. Mater.* **342**, 139 (2013).
- [23] H.J. Zhang *et al.*, *Sci. Rep.* **4**, 4844 (2014).
- [24] H.J. Zhang *et al.*, *Phys. Rev. Lett.* **114**, 166602 (2015).
- [25] A. Miyashita *et al.*, *Phys. Rev. B* **97**, 195405 (2018).
- [26] A. Miyashita *et al.*, *Phys. Rev. B* **102**, 045425 (2020).
- [27] H. Li, M. Maekawa, A. Miyashita, A. Kawasuso, *Defect and Diffusion Forum* **373**, 65 (2017).
- [28] A.C.L. Jones *et al.*, *Phys. Rev. Lett.* **114**, 153201 (2015).
- [29] A.C.L. Jones *et al.*, *Phys. Rev. Lett.* **117**, 216402 (2016).
- [30] P. Moskal *et al.*, *Nat. Commun.* **12**, 5658 (2021).
- [31] P. Moskal *et al.*, *Sci. Adv.* **7**, (2021).
- [32] K. Dulski *et al.*, *Nucl. Inst. Meth. Phys. Res. A* **1008**, 165452 (2021).